DFT and time-resolved IR investigation of electron transfer between photogenerated 17- and 19-electron organometallic radicals[†]

James F. Cahoon,[‡] Matthias F. Kling,[‡,§] Karma R. Sawyer,[‡] Lars K. Andersen,[**††] and Charles B. Harris[‡,*]

Department of Chemistry, University of California, Berkeley, California 94720, and Chemical Sciences Division and Physical Biosciences Division, MS Calvin Laboratory, Lawrence Berkeley National Laboratory, Berkeley, California 94720

* corresponding author. E-mail address: cbharris@berkeley.edu

---

[†] Part of the special issue in honor of F. Albert Cotton
[‡] University of California and Chemical Sciences Division, LBNL.
[§] Present address: Max Planck Institute of Quantum Optics, Hans-Kopfermann-Strasse 1, 85748 Garching, Germany.
[**] Physical Biosciences Division, LBNL
[††] Present address: European Commission, DG Research-JRC-IE Petten, Westerduinweg 3, Petten, The Netherlands.

ABSTRACT

The photochemical disproportionation mechanism of $[CpW(CO)_3]_2$ in the presence of Lewis bases PR_3 was investigated on the nano- and microsecond time-scales with Step-Scan FTIR time-resolved infrared spectroscopy. 532 nm laser excitation was used to homolytically cleave the W–W bond, forming the 17-electron radicals $CpW(CO)_3$ and initiating the reaction. With the Lewis base PPh_3, disproportionation to form the ionic products $CpW(CO)_3PPh_3^+$ and $CpW(CO)_3^-$ was directly monitored on the microsecond time-scale. Detailed examination of the kinetics and concentration dependence of this reaction indicates that disproportionation proceeds by electron transfer from the 19-electron species $CpW(CO)_3PPh_3$ to the 17-electron species $CpW(CO)_3$. This result is contrary to the currently accepted disproportionation mechanism which predicts electron transfer from the 19-electron species to the dimer $[CpW(CO)_3]_2$. With the Lewis base $P(OMe)_3$ on the other hand, ligand substitution to form the product $[CpW(CO)_2P(OMe)_3]_2$ is the primary reaction on the microsecond time-scale. Density Functional Theory (DFT) calculations support the experimental results and suggest that the differences in the reactivity between $P(OMe)_3$ and PPh_3 are due to steric effects. The results indicate that radical-to-radical electron transfer is a previously unknown but important process for the formation of ionic products with the organometallic dimer $[CpW(CO)_3]_2$ and may also be applicable to the entire class of organometallic dimers containing a single metal-metal bond.

KEYWORDS: 19-Electron intermediates; Transition-metal dimers; Metal-centered radicals; Electron transfer; Cage effects; Step-scan FTIR spectroscopy

1. Introduction

The reactivity of organometallic radicals is an important and ongoing question; odd-electron transition-metal species are used as synthetic precursors for more complex organometallic compounds and have also been shown to participate in important catalytic and electron-transfer reactions [1,2]. 17-electron (17e) metal-centered radicals are the most common transition-metal radicals and can be photochemically generated from organometallic dimers containing a single metal-metal bond; irradiation of $[CpW(CO)_3]_2$, $[CpFe(CO)_2]_2$, and $[Mn(CO)_5]_2$ produces the 17e radicals $CpW(CO)_3$, $CpFe(CO)_2$, and $Mn(CO)_5$, respectively [1]. Despite intense study of these prototypical dimers over several decades [1,3,4], they continue to yield surprising and new results. As early as 1968, dimers of the type $[CpM(CO)_3]_2$ (M = Mo, W) were observed to undergo photochemical disproportionation reactions in the presence of Lewis bases PR_3 to produce the ionic products $CpM(CO)_3^-$ and $CpM(CO)_3PR_3^+$ [5]. The mechanism of this unique reaction was analyzed and evidence was found for the existence of a highly reactive 19-electron (19e) radical, $CpM(CO)_3PR_3$ [6-8]. These same dimers were also observed to participate in ligand substitution reactions to produce the products $[CpM(CO)_2PR_3]_2$ or $[CpM(CO)_3][CpM(CO)_2PR_3]$, and again a 19e intermediate (or transition state) was postulated in these reactions [9].

Insert Scheme 1 approximately here

We recently used time-resolved infrared spectroscopy on the femto- through microsecond time-scales to probe the photochemical reactions of the dimer $[CpW(CO)_3]_2$ and directly observed the formation and the reactions of the 19e intermediate, $CpW(CO)_3PR_3$, for the first time [10-12]. In the Lewis base, $PR_3 = P(OMe)_3$, two main reaction pathways for 19e intermediates were found: ligand substitution and ultrafast in-cage disproportionation. The ultrafast disproportionation mechanism is displayed in Scheme 1. Irradiation of $[CpW(CO)_3]_2$

(**A**) at visible wavelengths results in metal-metal bond homolysis to form two 17e radicals, $CpW(CO)_3$ (**B**). The nascent radicals are surrounded by a cage of solvent molecules, represented by brackets in Scheme 1. Coordination of $P(OMe)_3$ with **B** forms the 19e species $CpW(CO)_3P(OMe)_3$ ($\mathbf{C_1}$) and electron transfer from $\mathbf{C_1}$ to **B** can form the disproportionated products $CpW(CO)_3P(OMe)_3^+$ ($\mathbf{D_1}$) and $CpW(CO)_3^-$ (**E**) while the radicals are in close proximity. The amount of ultrafast disproportionation is limited by the escape of the radicals from the solvent cage, preventing electron transfer. A delicate interplay between the formation rate of 19e species and the time-scale for diffusional separation of the radicals (approximately 140 ps for $P(OMe)_3$ / CH_2Cl_2 solutions) determines the precise yield of disproportionated products on the ultrafast time-scale [11]. In a given solvent, the branching ratio between reactions in- and outside of the initial solvent cage can be controlled via the reactivity of the Lewis base and the Lewis base concentration.

In low concentrations of the Lewis base $P(OMe)_3$, disproportionation is a minor pathway and 19e intermediates are instead found to undergo ligand substitution on the nanosecond time-scale [12] (see Scheme 2): the 19e species $\mathbf{C_1}$ loses a carbonyl to form the 17e species $CpW(CO)_2P(OMe)_3$ (**F**). Species **F** then dimerizes to form the ligand substitution product $[CpW(CO)_2P(OMe)_3]_2$ (**G**) on the microsecond time-scale. Note that the high reactivity of the 19e intermediates prevented direct observation of their reactions in many of the earlier studies on these types of organometallic dimers.

Insert Scheme 2 approximately here

Disproportionation may also occur on time-scales beyond the lifetime of the initial solvent cage. A reaction mechanism for disproportionation that was proposed by Tyler et al. [7,8] is shown in Scheme 3: electron transfer from **C** to the dimer **A** produces the cationic disproportionated product **D** and a negatively charged dimer $[CpW(CO)_3]_2^-$; homolysis of this

dimer generates the second disproportionated product **E** and an additional 17e radical **B**. Unlike the mechanism depicted in Scheme 1, disproportionation by Tyler's mechanism is rate-limited by diffusional encounter of the 19e species **C** and the dimer **A**. . Accordingly, disproportionation by this mechanism may take place on diffusion-limited time-scales, i.e. nanoseconds to microseconds. Hereafter, this mechanism will be referred to as the "dimer mechanism"

Insert Scheme 3 approximately here

In this paper, we present time-resolved infrared results for the photochemisty of $[CpW(CO)_3]_2$ with the Lewis base PPh_3. Unlike $P(OMe)_3$, we *do* observe significant disproportionation on diffusion-limited time-scales, but we find no evidence for the dimer mechanism (Scheme 3). Instead, the disproportionation kinetics can be explained by a mechanism similar to Scheme 1: electron transfer between an encounter-complex of the 19e species **C** and the 17e radical **B**. From here on this mechanism is referred to as the "radical mechanism". We present evidence for a similar (but minor) electron transfer pathway in high concentrations of the Lewis base $P(OMe)_3$ and give explanations for the large difference in reactivity between $P(OMe)_3$ and PPh_3. We also compare our results to the literature and suggest that the dimer mechanism may be a viable mechanism under certain reaction conditions (e.g. low intensity continuous irradiation) whereas the radical mechanism is operating for the experimental conditions described herein.

The paper is organized as follows: Section 2 provides a brief account of our experimental technique and theoretical approach, Section 3 presents the time-resolved results and addresses the possible disproportionation mechanisms. Our conclusions are summarized in Section 4.

2. Methods

2.1. Samples

$[CpW(CO)_3]_2$, trimethyl phosphite ($P(OMe)_3$), and triphenylphosphine (PPh_3) were

obtained from Sigma-Aldrich Co. and spectroscopic grade CH_2Cl_2 was purchased from EMD Chemicals. All samples were used without further purification. Air sensitive materials were stored and handled under nitrogen atmosphere in a glove-box (Vacuum Atmospheres Company). Air and light-sensitive solutions were continuously purged with argon and rigorously secluded from all ambient light sources.

2.2. Step-scan FTIR Spectroscopy

The experimental setup of the Step-scan apparatus has been described in detail elsewhere [13]. For experiments in the 1700 – 2100 cm^{-1} region, a HgCdTe PV detector KMPV8-1-J2 (fwhm = 37 ns, RC decay of AC amplifier = 1.4 ms) was employed. AC-coupled and DC-coupled interferometric signals were simultaneously acquired by a 40 MHz 12 bit digitizer (model PAD 1232). Samples were photolyzed with 25 ns pulses of the second harmonic of a Nd:YAG laser (DCR2A, GCR-3 optics) at 532 nm. Photolysis light was aligned in a nearly collinear geometry (10°) with the infrared beam. To prevent scattered 532 nm light from reaching interferometer and detector optics, Germanium plates (95% transmittance, anti-reflection coated) were placed in the openings of the interferometer and detector compartments. Data acquisition was triggered by a small fraction of the photolysis laser pulse detected with an EG&G Silicon photodiode (SGD-444). The sample, under Ar atmosphere, is flowed through a cell (Harrick Scientific) fitted with 1.5 mm thick CaF_2 or MgF_2 windows, giving an optical path length of 390 μm. Data was typically averaged over 15 laser-induced decays recorded for each mirror position of the Step-scan apparatus and 5-10 full time resolved Step-scan experiments were performed on each sample to ensure reproducibility and allow statistical analysis of data. Typically, changes in optical density of $\Delta OD = 5\times10^{-5}$ can be resolved in these experiments.

2.3. Data Analysis.

Kinetic data were derived from the spectral data at numerous times after photolysis. The

absorbance values within distinct spectral ranges for the various chemical species were averaged at each individual time delay. The ranges for each species were as follows: $CpW(CO)_3^-$ 1750–1800 cm^{-1}, $CpW(CO)_2P(OMe)_3$ 1815–1816 cm^{-1}, $CpW(CO)_3P(OMe)_3$ 1850–1860 cm^{-1}, $CpW(CO)_3(P(OMe)_3)_2^+$ 1980–2000 cm^{-1}, $CpW(CO)_2P(OMe)_3^-$ 1700–1730 cm^{-1}. Kinetic traces were then fit to various functions as noted in the text, and in all cases the functions included a floating parameter for time zero and a floating parameter for a constant vertical offset necessary to account for a small nonzero baseline in the experimental data. All reported errors correspond to 95% confidence intervals except where noted.

2.4. Theoretical.

Density functional theory (DFT) calculations have been performed to assist in the characterization of the various intermediate species and to facilitate an understanding of the dynamical behavior. Density functionals of the type used in this work have been shown to yield reliable results in calculations for transition-metal complexes [14].

DFT calculations were carried out using the program package Gaussian 03 [15], and the B3LYP hybrid method [16] was used in all calculations. It is composed of Becke's three-parameter exchange-functional [17] and the Lee-Yang-Parr non-local correlation functional [18]. Generic basis sets used consisted of the double-zeta LANL2DZ in conjunction with the relativistic effective core potential (ECP) of Hay and Wadt [19] for tungsten and 6-31G(d) (**I**) or 6-31G+(d) (**II**) basis sets for all other atoms. The Hessian matrices were calculated at the stationary points in order to ensure that true minima on the potential energy hypersurfaces had been found. Harmonic vibrational frequencies, appropriately scaled [20], are used in the spectral analysis of the experimental data. The electronic energies of all the optimized structures are within ca. 10 kcal/mol. For these open-shell complexes, the changes in energy are within a reasonable margin of error for these types of calculations. Thus, we do not use the energetics but

rather the vibrational frequencies and molecular geometries for the interpretation of the experimental results.

3. Results and Discussion

3.1. Reactions with PPh_3: Spectral Data.

The time-resolved infrared results for 1.0 mM $[CpW(CO)_3]_2$ (**A**) with 1.0 M PPh_3 in CH_2Cl_2 after photolysis at 532 nm are presented in Fig. 1 (see the supplementary material for spectra in neat CH_2Cl_2). Negative absorptions, or bleaches, result from the depletion of reactant molecules while positive absorptions correspond to the formation of intermediates and products after photolysis. Peak assignments are based on literature values [10,11,21]. Two bleaches from the *anti* conformation of $[CpW(CO)_3]_2$ (*anti*-**A**) are observed at 1907 and 1954 cm^{-1} and two peaks from the 17e radical $CpW(CO)_3$ (**B**) are observed at 1994 and 1881 cm^{-1}. A portion of the 17e radicals **B** dimerize to reform **A** in both the *anti* and *gauche* conformations:

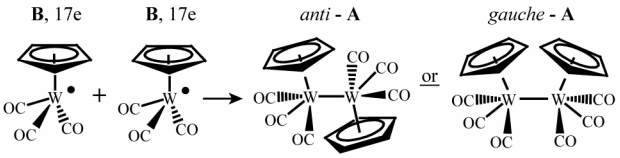

(1)

Formation of *anti*-**A** results in recovery of the bleach at 1954 cm^{-1} while the bleach at 1907 cm^{-1} maintains an approximately constant intensity due to spectral overlap with the peak from **B** at 1881 cm^{-1}. The formation of *gauche*-**A**, on the other hand, causes the rise of an absorption at 2010 cm^{-1} in Fig. 1a. Isomerization of the *gauche* isomer to the more stable *anti* isomer may occur, although the free energy of activation has been estimated at 16.2 ± 0.5 kcal/mol [22]. Isomerization would thus take place on the time-scale of milliseconds to seconds and is not observed in these experiments on the microsecond time-scale.

Insert Fig. 1 approximately here

The 17e radicals (**B**) which do not dimerize to reform **A** are in equilibrium with 19e

species $CpW(CO)_3PPh_3$ (**C_2**) which exhibit an absorption at 1855 cm^{-1}. This assignment is based on our previous ultrafast studies on this dimer complex and is in accord with the DFT calculations contained in Table 1. The 17e and 19e radicals disproportionate to form the ionic products $CpW(CO)_3^-$ (**E**) and $CpW(CO)_3PPh_3^+$ (**D_2**). Peaks from **E** appear at 1768 and 1795 cm^{-1} and a single peak from **D_2** appears at 2055 cm^{-1} in Fig. 1. It has been proposed that on the microsecond time-scale, disproportionation might occur via the mechanism depicted in Scheme 3 (dimer mechanism) and discussed in the Introduction. The central feature of this mechanism is electron transfer from the 19e species **C** to the dimer **A** to form the products **D** and $[CpW(CO)_3]_2^-$; however, we find no absorption attributable to $[CpW(CO)_3]_2^-$ (see Table 1 for the calculated frequencies of this species). This finding does not conclusively discard the dimer mechanism (Scheme 3) since $[CpW(CO)_3]_2^-$ may be a short-lived intermediate which never builds-up sufficient concentration to be detected in our experiment.

Insert Table 1 approximately here

We propose here an alternative disproportionation mechanism (radical mechanism), which we will test against the dimer mechanism: the disproportionated products are directly formed by electron transfer from the 19e species **C** to the 17e radical **B**, similar to Scheme 1:

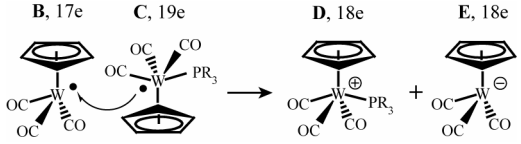

(2)

Unlike Scheme 1, however, the radical pair is formed by diffusional encounter of species **B** and **C** rather than by homolysis of the metal-metal bond in **A**. In order to distinguish these two possible disproportionation mechanisms (the dimer and the radical mechanisms), we performed concentration dependent studies. The rate and extent of disproportionation by the dimer mechanism depends on concentration of dimer **A**, but disproportionation by the radical

mechanism should be independent of the dimer concentration. In addition, we varied the initial concentration of the 17e radical **B** by changing the 532 nm laser intensity. As will be shown in our kinetic analysis of the data, the two mechanisms are expected to depend on the concentration of radicals **B** in a different manner. For all the concentration dependent studies, we used a PPh_3 concentration of 85 mM. This low concentration prevented a significant amount of disproportionation from occuring on the picosecond time-scale.

First, data collected with different dimer concentrations lends some insight into the disproportionation mechanism. Data collected at a concentration of 1.5 mM **A** and at a concentration one-third lower, 0.5 mM **A**, are shown in Figs. 2a and 2b, respectively. Note that the concentration of **A** for the data presented in Fig. 2a (1.5 mM) is the same concentration used in the detailed studies by Tyler et al. and discussed in the Introduction [7]. The initial radical **B** concentration (at 1 μs) in the experiments with the two concentrations of **A** was kept constant by using a higher laser intensity for the 0.5 mM solution [23]. Qualitative comparison between Figs. 2a and 2b reveals no significant difference between the two data sets. This initial result lends support to the radical mechanism, which is expected to be independent of the dimer **A** concentration.

Insert Fig. 2 approximately here.

Additional insight into the mechanism is provided by data collected at the same concentration of dimer **A** (here 1.5 mM) but with different initial concentrations of the 17e radical **B** (Fig. 2c shows the data for an approximately 2.5 times greater concentration of **B** as compared to Fig. 2a). For a higher **B** concentration the disproportionation yield is significantly enhanced (as can be seen by the larger relative intensity of the disproportionation peaks (**D_2**, **E**) in Fig. 2c as compared to Fig. 2a; note the change in the ordinate scale). As both the dimer and the radical mechanism predict this type of behavior, further conclusions require a detailed kinetic

analysis that is given in the following section.

3.2. Reactions with PPh_3: Kinetic Analysis.

In the kinetic modeling of the experimental data, we will first make a few simplifying yet physically reasonable assumptions. We assume that the concentrations of the dimer $[CpW(CO)_3]_2$ (**A**) and the Lewis base PPh_3 remain constant within the time-scale of the experiment. For the data presented in Fig. 2a, laser photolysis depletes less than 3% of the dimer molecules within the volume of sample irradiated by one laser pulse and depletes less than 5% of the total dimer concentration during the course of the experiment [24]. The concentration of PPh_3 is far greater than the dimer concentration and so is negligibly changed by the photochemical reactions. Furthermore, in agreement with the kinetic analysis by Scott et al. [25], the 17e and 19e species are assumed to be in equilibrium with the equilibrium constant K_{eq}:

$$CpW(CO)_3\ (\mathbf{B}) \ + \ PPh_3 \ \overset{K_{eq}}{\rightleftharpoons} \ CpW(CO)_3PPh_3\ (\mathbf{C_2}), \tag{3}$$

and the equilibrium lies far on the side of the 17e species ($K_{eq} = 6 \pm 1\ M^{-1}$) [25].

The two alternative pathways that may yield disproportionation on diffusion-limited time-scales, the radical and the dimer mechanisms, are represented in eqs. 4 and 5, respectively:

$$CpW(CO)_3\ (\mathbf{B}) \ + \ CpW(CO)_3PPh_3\ (\mathbf{C_2}) \ \overset{k_4}{\rightarrow} \ CpW(CO)_3P(OMe)_3^{+}\ (\mathbf{D_1}) \ + \ CpW(CO)_3^{-}\ (\mathbf{E}) \tag{4}$$

$$[CpW(CO)_3]_2\ (\mathbf{A}) \ + \ CpW(CO)_3PPh_3\ (\mathbf{C_2}) \ \overset{k_5}{\rightarrow}$$

$$CpW(CO)_3PPh_3^{+}\ (\mathbf{D_1}) \ + \ CpW(CO)_3^{-}\ (\mathbf{E}) \ + \ CpW(CO)_3\ (\mathbf{B}) \tag{5}$$

Eq. 6 describes the dimerization of two 17e radicals to reform the parent dimer **A**:

$$CpW(CO)_3\ (\mathbf{B}) \ + \ CpW(CO)_3\ (\mathbf{B}) \ \overset{k_6}{\rightarrow} \ [CpW(CO)_3]_2\ (\mathbf{A}). \tag{6}$$

From eqs. 3, 5, and 6 and the assumptions given above, we can now derive an equation for the concentrations of the disproportionated products $\mathbf{D_2}$ and **E** for the *dimer mechanism*:

$$[\mathbf{D_2}] = [\mathbf{E}] = \frac{k_5}{k_6}[PPh_3][\mathbf{A}]K_{eq}\ln(k_6[\mathbf{B}]_0 t + 1)\ , \tag{7}$$

where t is time and $[\mathbf{B}]_0$ is the concentration of the 17e radicals **B** at time $t = 0$. A similar analysis may be performed for the *radical mechanism* using eqs. 3, 4 and 6:

$$[\mathbf{D_2}] = [\mathbf{E}] = \frac{k_4 K_{\mathrm{eq}}[\mathrm{PPh_3}]}{k_4 K_{\mathrm{eq}}[\mathrm{PPh_3}] + k_6} \left(\frac{-1}{\left(k_4 K_{\mathrm{eq}}[\mathrm{PPh_3}] + k_6\right) t + [\mathbf{B}]_0^{-1}} + [\mathbf{B}]_0 \right), \tag{8}$$

A comparison of eqs. 7 and 8 shows that the two disproportionation mechanisms are expected to exhibit different kinetic behavior. The dimer mechanism should show logarithmic behavior (eq. 7) while the radical mechanism should be consistent with a function of the form $-1/t$ (eq. 8). The experimental kinetic data for the anionic disproportionated product **E** from Fig. 2a is shown in Fig. 3a and fits to eqs. 7 and 8 are displayed as the red and blue lines, respectively (see the supplementary material for details of the fitting procedure and the fitting parameters for the cationic and anionic disproportionated products ($\mathbf{D_2}$, **E**) for all concentrations of **A** and **B**). Even when taking the noise in the data into account, examination of these fits shows that the functional form of eq. 8 provides a better fit to the experimental data.

Insert Fig. 3 approximately here

If disproportionation follows the radical mechanism, in a plot of $1/(\Delta\mathrm{mOD} - \mathrm{A})$ over time t, where A is the long-time limit of the disproportionation concentration (the asymptote in Fig. 3a), the data will follow a straight line. Such a representation of the data is given in Fig. 3b together with the best fits from the radical (blue line) and the dimer mechanism (red line). Within experimental noise, the data appear to follow the linear behavior predicted by the radical mechanism. The values of fits to the data presented in Fig. 2 are given in the supplementary material. Starting from the analysis of a particular set of **A** and **B** concentrations, we can now predict the yield of disproportionated product which would be expected from each mechanism as the dimer concentration and initial radical concentrations are varied. In Table 2 we compare the experimental data for the relative absorption of species **E** at distinctly chosen concentrations of

A and **B** with the values predicted by the two mechanisms from eqs. 7 and 8. The data are normalized to data set (a) because this data set is used to establish the best fit parameters. For data set (b), the dimer concentration has been decreased by one-third, and because disproportionation by the dimer mechanism depends on the presence of dimer molecules, this mechanism predicts a sharp decrease in the disproportionation yield. The radical mechanism, on the other hand, predicts a slight increase in the disproportionation yield because there was a slight increase in the initial concentration of the radical **B**. The experimental data are clearly in agreement with the prediction of the radical mechanism since the disproportionation yield marginally increases in comparison to data set (a). For data set (c), the laser photolysis power was significantly increased to augment the initial concentration of the radical **B** [23]. The dimer mechanism predicts a small increase in the disproportionation yield while the radical mechanism predicts a far more dramatic increase. Again, the radical mechanism provides a better predication of the experimentally observed disproportionation yield.

Insert Table 2 approximately here

3.3. Disproportionation mechanism with PPh_3

Our experimental results and the kinetic modeling for the photochemical disproportionation of $[CpW(CO)_3]_2$ (**A**) with PPh_3 provide the following evidence for the reaction mechanism. First, we find no spectroscopic evidence for $[CpW(CO)_3]_2^-$, a key intermediate in the dimer disproportionation mechanism. Second, the kinetics of disproportionation are more consistent with the kinetic model derived for the radical mechanism than for the dimer mechanism. Third, changes in the yield of disproportionated products with changing concentrations of dimer **A** and radical **B** show poor agreement with the dimer mechanism but are consistent with the radical mechanism - specifically, when the dimer concentration was reduced by one-third, the disproportionation yield increased, the opposite

result predicted from the dimer mechanism but the correct result according to the radical mechanism. Based on these findings, we conclude that on diffusion-limited time-scales disproportionation in PPh_3 is more appropriately described with the radical mechanism. In Section III D, we provide alternative explanations for evidence in the literature in favor of the dimer mechanism.

Insert Scheme 4 approximately here

The complete mechanism for photochemical disproportionation of $[CpW(CO)_3]_2$ (**A**) with the Lewis base PPh_3 on ultrafast and diffusion-limited time-scales is summarized in Scheme 4. Photolysis of **A** at visible wavelengths produces two 17e radicals **B** surrounded by a cage of solvent molecules, represented by brackets in Scheme 4. These radicals may follow two different pathways; coordination of PPh_3 with one 17e radical may form a 19e radical $\mathbf{C_2}$ and cause disproportionation inside the initial solvent cage within hundreds of picoseconds after photoexcitation. Alternatively, the 17e radicals **B** may escape the solvent cage. A portion of the 17e radicals **B** which escape the initial solvent cage will recombine at a diffusion-limited rate to reform the dimer **A** (not shown in Scheme 4). The remaining radicals, as depicted in Scheme 4, may react with PPh_3 to form a 19e radical $\mathbf{C_2}$. These 19e radicals may then encounter remaining 17e radicals at a diffusion controlled rate and form an encounter complex analogous to the solvent caged complex directly after photolysis. The 17e and 19e radicals in the encounter complex can then disproportionate to form the final products $\mathbf{D_2}$ and **E**.

3.4. Reactions with $P(OMe)_3$

We recently reported nano- and microsecond time-resolved infrared results for the photochemistry of $[CpW(CO)_3]_2$ (**A**) with a relatively low concentration of Lewis base $P(OMe)_3$ (85 mM in CH_2Cl_2). As discussed in the Introduction, we directly observed spontaneous CO loss from the 19e species $CpW(CO)_3P(OMe)_3$ ($\mathbf{C_1}$) to form the 17e species $CpW(CO)_2P(OMe)_3$

($\mathbf{F_1}$) (refer to Scheme 2). Species $\mathbf{F_1}$ subsequently dimerizes to form the ligand substitution product $[CpW(CO)_2P(OMe)_3]_2$ (**G**). Here, we present results at a higher concentration (1 M) of the Lewis base $P(OMe)_3$. While ligand substitution is still the primary reaction at this higher concentration, we also find evidence for a new radical-to-radical electron transfer reaction.

Nano- and microsecond time-resolved results for a 1 M concentration of $P(OMe)_3$ in CH_2Cl_2 with 1.5 mM **A** are presented in Fig. 4. Similar to Fig. 1, peaks from the *anti* isomer of **A** appear at 1901 and 1955 cm^{-1}, and peaks from the 17e radical $CpW(CO)_3$ (**B**) appear at 1880 and 1994 cm^{-1}. Two peaks from the 19e species $CpW(CO)_3P(OMe)_3$ ($\mathbf{C_1}$) are apparent at 1854 cm^{-1} and 1967 cm^{-1} [10,11]. In accord with our previous results, the 19e species $\mathbf{C_1}$ loses a carbonyl on the nanosecond time-scale (Fig. 4a) to form the 17e species $\mathbf{F_1}$, with peaks at 1815 and 1916 cm^{-1} [12,26]. The net reaction from the 17e **B** to 17e $\mathbf{F_1}$ is an associative ligand substitution, a reaction commonly observed with organometallic radicals [9,27]. The spontaneous loss of a carbonyl from the 19e complex is also consistent with the reactivity observed after electrochemical reduction of similar types of complexes [28-30]. Kinetics for this process are depicted in Fig. 5a and exhibit single exponential behavior according to the following equation:

$$[\mathbf{C_1}] = [\mathbf{C_1}]_0 \, e^{\frac{-k_{diss}t}{1+(K_{eff}[P(OMe)_3])^{-1}}}, \qquad (9)$$

where $[\mathbf{C_1}]_0$ is the initial concentration of $\mathbf{C_1}$, k_{diss} is the rate constant for CO dissociation from $\mathbf{C_1}$, K_{eff} is the effective $\mathbf{B}/\mathbf{C_1}$ equilibrium constant, $[P(OMe)_3]$ is the Lewis base concentration, and t is time. The time constant from a monoexponential fit to the kinetics of $\mathbf{C_1}$ (see Fig. 5a) gives $\tau = 81 \pm 8$ ns. In agreement with eq. 9 we find this time to be shorter compared to an 85 mM $P(OMe)_3$ concentration ($\tau = 280 \pm 9$ ns) [12]. As expected, the rise of $\mathbf{F_1}$ is directly correlated with the decay of $\mathbf{C_1}$ and gives a time constant of $\tau = 70 \pm 5$ ns.

Insert Fig. 4 approximately here.

On the microsecond time-scale, peaks from the ligand substitution product **G,** resulting from dimerization of the 17e species $\mathbf{F_1}$, appear at 1835 and 1868 cm^{-1} (refer to Scheme 2). To our surprise, we also observed two additional peaks at 1990 and 1714 cm^{-1}, labeled **H** and **I** in Fig. 4b, respectively. Kinetics for these peaks are displayed in Fig. 5b and monoexponential fits to these kinetic traces yield rise times of 43 ± 7 μs and 45 ± 5 μs for **H** and **I**, respectively. We propose that these peaks arise from the ionic products $CpW(CO)_2(P(OMe)_3)_2^+$ (**H**) and $CpW(CO)_2P(OMe)_3^-$ (**I**). DFT calculations for the harmonic frequencies of these species are contained in Table 1. The calculations predict a shift in CO stretching frequency from the 17e radical $CpW(CO)_2P(OMe)_3$ ($\mathbf{F_1}$) to the new ionic product $CpW(CO)_2P(OMe)_3^-$ (**I**) of 94 cm^{-1}, which is in good agreement with the experimental shift of 101 cm^{-1}. Similarly, a shift from the disproproportionated product $CpW(CO)_3P(OMe)_3^+$ ($\mathbf{D_1}$) to the new ionic product $CpW(CO)_2(P(OMe)_3)_2^+$ (**H**) of 84 cm^{-1} is predicted, in reasonable agreement with the experimental shift of 74 cm^{-1}.

Insert Fig. 5 approximately here

The simplest explanation for the formation of **H** and **I** is electron transfer between two 17e radicals $CpW(CO)_2P(OMe)_3$ ($\mathbf{F_1}$) with concomitant coordination of a second Lewis base to the electron donor, as shown in equation 10:

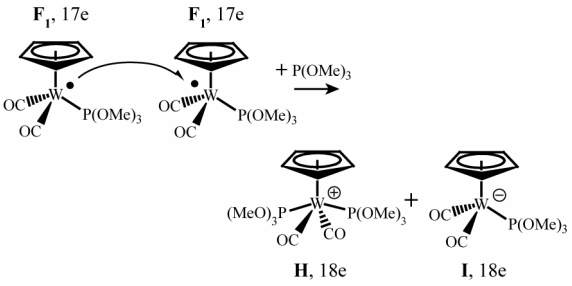

(10)

Although it is conceivable for electron transfer between the radicals to occur without coordination of the Lewis base, this reaction would produce the 16-electron (16e) cation

$CpW(CO)_2P(OMe)_3^+$, which is coordinatively unsaturated and likely subject to back electron transfer, reproducing the 17e radicals. In addition, we have found no spectroscopic evidence for the formation of a 16e cation. Thus, it is more probable that photoproducts **H** and **I** are formed by concerted electron transfer and coordination of $P(OMe)_3$. This trimolecular process should only produce an appreciable yield in high concentrations of $P(OMe)_3$, which explains the absence of these products at a lower 85 mM concentration [12]. This result emphasizes the importance of radical-to-radical electron transfer in the formation of ionic products with $[CpW(CO)_3]_2$. Note that the formation of $CpW(CO)_2P(OMe)_3^-$ (**I**) cannot be explained by electron transfer from the 19e species $\mathbf{C_1}$ to the dimer **A** because this reaction would produce $CpW(CO)_3^-$ (**E**) rather than **I**.

3.5. Comparison of Lewis base reactivity

The time-resolved infrared results presented herein indicate that the formation of ionic products in the photochemistry of $[CpW(CO)_3]_2$ (**A**) with Lewis bases results from electron transfer between radical species. The results also show that on diffusion-limited time-scales, ligand substitution is the primary reaction channel for the 19e species $CpW(CO)_3PR_3$ when R = OMe but disproportionation is the primary reaction when R = Ph. A natural question arises: what causes the sudden change in reactivity between these two Lewis bases?

At first glance, CO loss from the sterically crowded 19e species $CpW(CO)_3PPh_3$ ($\mathbf{C_2}$) would appear to be a favorable process in comparison to CO loss from the less sterically crowded 19e species $CpW(CO)_3P(OMe)_3$ ($\mathbf{C_1}$), yet this is not the result observed experimentally. Cone-angle is the generally accepted size of a coordinating ligand, and the Lewis base PPh_3 possesses a cone angle of 145° while $P(OMe)_3$ is dramatically smaller at only 107° [31]. Thus, the 19e species with R = Ph would be expected to experience far greater steric strain than the R = OMe counterpart.

Insert Fig. 6 approximately here

The DFT optimized structures of the 19e species (**C**) as well as the CO loss 17e species (**F**) for both R = OMe and R = Ph are illustrated in Fig. 6. Perhaps the most striking result is that upon CO loss the W–P bond distance decreases by 0.23 Å for R = OMe while the bond distance decreases by only 0.03 Å for R = Ph. Qualitatively, the driving force for CO loss with R = OMe appears to be a stronger W–P bond while this driving force does not exist for R = Ph. In addition, the 17e CO-loss radical with the less sterically demanding Lewis base $P(OMe)_3$ achieves a W–P bond distance 0.09 Å shorter than with the more sterically hindered PPh_3 counterpart. This result further supports that CO loss is more favorable with the smaller $P(OMe)_3$ Lewis base.

A comparison of the 19e structures for both R = OMe and R = Ph in Fig. 6a and 6c shows that the sterically encumbered R = Ph system achieves, surprisingly, a W–P bond distance 0.11 Å shorter than the R = OMe analog. In addition, the C–W–C bond angle for opposite CO groups is approximately 45° larger with R = Ph. Based on these calculations alone, it is difficult to determine the reason for these differences in molecular structure. To provide additional insight, we performed calculations on analogous 19e species with R = Me and R = Bu (Me = CH_3; Bu = $(CH_3)_3CH_4$), and the structures are shown in Fig. 7. The Lewis bases PMe_3 and PBu_3 have nearly identical electronic properties but are of extremely different sizes; any differences in structure between the two 19e species are the result of steric effects. The W–P bond distance with R = Bu is 0.21 Å shorter than with R = Me, and the C-W-C bond angle of opposite CO groups is 44° larger than with R = Me. These phospines thus reproduce the same trend as observed with R = OMe and Ph; the bulkier Lewis base distorts the structure of the CO groups, and apparently, this steric effect permits a shorter W–P bond distance in the 19e species. The similarity of the Me/Bu structures with OMe/Ph structures suggest that the differences observed between R = OMe and R = Ph are entirely attributable to steric effects.

Insert Fig. 7 approximately here.

3.6 Comparison to mechanistic conclusions from previous studies

The dimer mechanism for disproportionation is often cited in the literature, yet the time-resolved infrared measurements presented in this paper provide no evidence in support of the dimer mechanism when the reaction is initiated by intense pulsed laser irradiation. Instead, disproportionation appears to proceed by the radical mechanism: electron transfer between the 19e and 17e radicals. When Tyler and co-workers originally proposed the dimer mechanism more than twenty years ago [7,8], the novel aspect of the mechanism was the possibility of a 19e radical which serves as a strong reductant and initiates electron transfer; this aspect has clearly been proven correct. We have demonstrated, however, that the 17e radical rather than the dimer appears to be the electron acceptor for the reaction conditions present in our experiments. The idea that disproportionation proceeds by a mechanism involving electron transfer from a radical to the parent dimer has been well addressed in the literature and originated from Brown and co-workers studies on Co and Mn carbonyl dimers [32-35]. There is considerable evidence for this type of mechanism; thus, we suggest that electron transfer from the 19e species to the parent dimer is a viable though less favorable reaction pathway in comparison to electron transfer from the 19e species to 17e radical. In cases where 17e radicals are in extremely low concentrations or are rendered poor electron acceptors (e.g. due to substitution of CO for a more electron donating ligand), electron transfer from the 19e species to the parent dimer is the more likely reaction pathway. In the following section, we discuss the experimental evidence for the dimer mechanism and the conditions which may favor this mechanism.

The dimer mechanism as shown in Scheme 3 produces a new 17e radical **B** for every radical consumed in the disproportionation reaction; thus, disproportionation according to this mechanism is a self-sustaining chain process which continues until termination by radical-radical

recombination (eq. 6). In contrast, the radical mechanism we propose does not predict a chain mechanism because no additional radicals are generated by the disproportionation reaction. Tyler and co-workers advanced two main arguments to support disproportionation by electron transfer to the dimer. Note that Tyler's papers mainly address the photochemistry of $[CpMo(CO)_3]_2$ rather than the W analog studied here, but, as stated in their paper [7], they performed experiments on the W analog which led them to believe that in all cases the reactivity of the two dimers is the same.

First, in order to show that the anionic dimer $[MeCpMo(CO)_3]_2^-$ is a key intermediate which begins the radical chain mechanism (MeCp rather than Cp was used in their studies for solubility purposes), Tyler and co-workers directly produced this species by sodium metal reduction of the dimer $[MeCpMo(CO)_3]_2$ in the presence of the Lewis base $PPh_2(CH_3)$ and observed significant formation of the disproportionated product $(MeCp)Mo(CO)_3^-$ [7]. In the absence of Lewis base, they reported only small amounts of $(MeCp)Mo(CO)_3^-$. While this experiment does indicate that the anionic dimer would decompose to an anion and radical, the results may also be explained in light of our new results. Decomposition of the anionic dimer produces the 17e radical **B** in addition to the anion; a portion of the chemically generated 17e radicals will coordinate with the Lewis base $PPh_2(CH_3)$ to form 19e radicals. These 17e and 19e radicals may then disproportionate according to the radical mechanism. The radical mechanism does not, however, explain the quantum yields observed in these experiments, as discussed below.

The second major evidence for the dimer mechanism is a quantum yield greater than one for the disproportionation reactions of $[(MeCp)Mo(CO)_3]_2$ with a variety of phosphine and phosphite Lewis bases [7]. A quantum yield greater than one is a clear indication of a chain process and supports the dimer mechanism. Specifically, quantum yields greater than one were

reported for PPh_2CH_3, $P(OMe)_3$, and the bidentate ligand bis(1,2-diphenylphosphino)ethane (dppe). It is important to point out that these earlier photochemical studies were performed under continuous photolysis conditions which may change the reaction conditions in two important ways in comparison to the time-resolved experiments. First, continuous photolysis provides a lower power and light intensity compared to pulsed laser excitation. The relatively intense laser light may produce a high concentration of radicals which heavily favors radical-to-radical electron transfer and radical-radical termination. In this scenario, the dimer mechanism may occur at the low radical concentrations produced by continuous photolysis but be shut down at the higher concentrations produced by laser excitation. This scenario is also supported by previous studies of Tyler and co-workers which showed that an increase in light intensity leads to a decrease in disproportionation quantum yields [36], suggesting that radical-radical termination reactions prevail at higher light intensities. Note that a radical concentration sufficiently low to disfavor radical-radical chemistry would likely be undetectable given the signal-to-noise ratio in time-resolved IR experiments.

The second important difference between continuous and pulsed laser excitation is the possibility that an intermediate could absorb another photon. Our time-resolved infrared experiments allow only a single photon absorption since this one photochemical event defines time zero for the experiment. In contrast, a continuous photolysis experiment may allow the 19e species $CpW(CO)_3(PPh_2CH_3)$ to absorb a photon and quickly lose a carbonyl to form the 17e species $CpW(CO)_2(PPh_2CH_3)$ [12,37]. Such a photochemical reaction will quickly deplete the solution of 17e radicals $CpW(CO)_3$ and prevent disproportionation by the radical mechanism. The remaining radical species in solution, most likely both $CpW(CO)_2(PPh_2CH_3)$–(PPh_2CH_3) and $CpW(CO)_3(PPh_2CH_3)$, may undergo electron transfer to the dimer to produce disproportionated products. The rate for electron transfer to the dimer is in all likelihood far

slower than electron transfer to the 17e radical $CpW(CO)_3$, but this slower process will occur when the $CpW(CO)_3$ radicals are quickly eliminated or reduced to a low concentration given the reaction conditions. Similar arguments may be made for the Lewis bases $P(OMe)_3$ and dppe.

4. Summary and Conclusions

We have studied the photo-induced disproportionation reactions of $[CpW(CO)_3]_2$ with the Lewis bases $P(OMe)_3$ and PPh_3 on diffusion-limited time-scales using time-resolved infrared spectroscopy. Intense pulsed laser irradiation of $[CpW(CO)_3]_2$ homolytically cleaves the metal-metal bond to produce two 17e radicals $CpW(CO)_3$, and coordination of Lewis bases PR_3 to these radicals forms the 19e species $CpW(CO)_3PR_3$. A detailed analysis of the experimental data indicates that the subsequent formation of ionic products such as $CpW(CO)_3PR_3^+$ and $CpW(CO)_3^-$ proceeds by electron transfer from the 19e radicals to 17e radicals. This result is contrary to the currently accepted dimer mechanism for disproportionation which predicts electron transfer from the 19e radical to the parent dimer (Scheme 3). Disproportionation by the dimer mechanism likely occurs only when the 17e radicals are in extremely low concentration and thus not available to serve as the electron acceptor. This condition may arise in continuous photolysis experiments at low light intensities or in cases in which the 17e radicals are nearly all converted to 19e species.

The results presented in this paper offer the first evidence that radical-to-radical electron transfer is an important process on diffusion-limited time-scales for the photochemistry of organometallic dimers containing a single metal-metal bond. We believe these results are not only applicable to the dimers $[CpM(CO)_3]_2$ (M = Mo, W), but also to the dimers $[CpM(CO)_2]_2$ (M = Fe, Ru), $M_2(CO)_{10}$ (M = Mn, Re), and $M_2(CO)_8$ (M = Co, Rh) which have been observed to form similar ionic products in the presence of Lewis bases.

Acknowledgements. We thank Heinz Frei for the generous use of his Step-Scan FTIR apparatus and a reviewer for his viable comments on our manuscript. This work was supported by the NSF's Division of Physical Chemistry. We also acknowledge some specialized equipment supported by the U.S. Department of Energy Office of Basic Energy Sciences, Chemical Sciences Division, under contract DE-AC02-05CH11231 and contractor supported research. J.F.C acknowledges an NSF graduate research fellowship and M.F.K. is grateful for support by the Alexander von Humboldt foundation through a Feodor-Lynen Fellowship.

Supplementary Material: Spectral data recorded in neat CH_2Cl_2, and details of the analysis of the disproportionation kinetics.

References.

[1] M.C. Baird, Chem. Rev., 88 (1988) 1217.
[2] D. Astruc, Chem. Rev., 88 (1988) 1189.
[3] D.R. Tyler, Acc. Chem. Res., 24 (1991) 325.
[4] T.E. Bitterwolf, Coord. Chem. Rev., 211 (2001) 235.
[5] R.J. Haines, R.S. Nyholm and M.H. Stiddard, J. Chem. Soc. A., (1968) 43.
[6] A.E. Stiegman and D.R. Tyler, J. Am. Chem. Soc., 104 (1982) 2944.
[7] A.E. Stiegman, M. Stieglitz and D.R. Tyler, J. Am. Chem. Soc., 105 (1983) 6032.
[8] C.E. Philbin, A.S. Goldman and D.R. Tyler, Inorg. Chem., 25 (1986) 4434.
[9] N.N. Turaki and J.M. Huggins, Organometallics, 5 (1986) 1703.
[10] M.F. Kling, J.F. Cahoon, E.A. Glascoe, J.E. Shanoski and C.B. Harris, J. Am. Chem. Soc., 126 (2004) 11414.
[11] J.F. Cahoon, M.F. Kling, S. Schmatz and C.B. Harris, J. Am. Chem. Soc., 127 (2005) 12555.
[12] J.F. Cahoon, M.F. Kling, K.R. Sawyer, H. Frei and C.B. Harris, J. Am. Chem. Soc., 128 (2006) 3152.
[13] H. Sun and H. Frei, J. Phys. Chem. B, 101 (1997) 205.
[14] S.Q. Niu and M.B. Hall, Chem. Rev., 100 (2000) 353.
[15] M.J. Frisch, G.W. Trucks, H.B. Schlegel, G.E. Scuseria, M.A. Robb, J.R. Cheeseman, J.A. Montgomery, Jr., T.Vreven, K.N. Kudin, J.C. Burant, J.M. Millam, S.S. Iyengar, J. Tomasi, V. Barone, B. Mennucci, M. Cossi, G. Scalmani, N. Rega, G.A. Petersson, H. Nakatsuji, M. Hada, M. Ehara, K. Toyota, R. Fukuda, J. Hasegawa, M. Ishida, T. Nakajima, Y. Honda, O. Kitao, H. Nakai, M. Klene, X. Li, J.E. Knox, H.P. Hratchian, J.B. Cross, V. Bakken, C. Adamo, J. Jaramillo, R. Gomperts, R.E. Stratmann, O. Yazyev,

A.J. Austin, R. Cammi, C. Pomelli, J.W. Ochterski, P.Y. Ayala, K. Morokuma, G.A. Voth, P. Salvador, J.J. Dannenberg, V.G. Zakrzewski, S. Dapprich, A.D. Daniels, M.C. Strain, O. Farkas, D.K. Malick, A.D. Rabuck, K. Raghavachari, J.B. Foresman, J.V. Ortiz, Q. Cui, A.G. Baboul, S. Clifford, J. Cioslowski, B.B. Stefanov, G. Liu, A. Liashenko, P. Piskorz, I. Komaromi, R.L. Martin, D.J. Fox, T. Keith, M.A. Al-Laham, C.Y. Peng, A. Nanayakkara, M. Challacombe, P.M.W. Gill, B. Johnson, W. Chen, M.W. Wong, C. Gonzalez, J.A. Pople, Gaussian 03, Revision C.02, Gaussian, Inc., Wallingford, CT, 2004.

[16] P.J. Stephens, F.J. Devlin, C.F. Chabalowski and M.J. Frisch, J. Phys. Chem., 98 (1994) 11623.

[17] A.D. Becke, J. Chem. Phys., 98 (1993) 5648.

[18] C.T. Lee, W.T. Yang and R.G. Parr, Phys. Rev. B, 37 (1988) 785.

[19] P.J. Hay and W.R. Wadt, J. Chem. Phys., 82 (1985) 299.

[20] A.P. Scott and L. Radom, J. Phys. Chem., 100 (1996) 16502.

[21] I.G. Virrels, M.W. George, F.P.A. Johnson, J.J. Turner and J.R. Westwell, Organometallics, 14 (1995) 5203.

[22] R.D. Adams, D.M. Collins and F.A. Cotton, Inorg. Chem., 13 (1974) 1086.

[23] The bleach intensity increased approximately linearly with the laser intensity, indicating that the laser intensity was not so high as to cause two photon absorption.

[24] This number represents an upper limit based on a 1.0 quantum yield and neglecting any recombination of the 17e radicals. For data presented in Figures 2b and 2c, a greater portion of the dimer molecules within the sample volume may be consumed. This effect is not included in the yield analysis of the experimental data (see Figure 4) but would only increase the discrepancy between the dimer mechanism and experimental data, thus strengthening the arguments made in the section.

[25] S.L. Scott, J.H. Espenson and W.J. Chen, Organometallics, 12 (1993) 4077.

[26] T.S. Chong, P. Li, W.K. Leong and W.Y. Fan, J. Organomet. Chem., 690 (2005) 4132.

[27] A.J. Dixon, S.J. Gravelle, L.J. Vandeburgt, M. Poliakoff, J.J. Turner and E. Weitz, Journal of the Chemical Society-Chemical Communications, (1987) 1023.

[28] Y. Huang, C.C. Neto, K.A. Pevear, M.M.B. Holl, D.A. Sweigart and Y.K. Chung, Inorg. Chim. Acta, 226 (1994) 53.

[29] C.C. Neto, S. Kim, Q. Meng, D.A. Sweigart and Y.K. Chung, J. Am. Chem. Soc., 115 (1993) 2077.

[30] K.A. Pevear, M.M.B. Holl, G.B. Carpenter, A.L. Rieger, P.H. Rieger and D.A. Sweigart, Organometallics, 14 (1995) 512.

[31] C.A. Tolman, Chem. Rev., 77 (1977) 313.

[32] M. Absi-Halabi and T.L. Brown, J. Am. Chem. Soc., 99 (1977) 2982.

[33] M. Absi-Halabi, J.D. Atwood, N.P. Forbus and T.L. Brown, J. Am. Chem. Soc., 102 (1980) 6248.

[34] N.P. Forbus, R. Oteiza, S.G. Smith and T.L. Brown, J. Organomet. Chem., 193 (1980) C71.

[35] S.B. McCullen and T.L. Brown, Inorg. Chem., 20 (1981) 3528.

[36] A.E. Stiegman, A.S. Goldman, C.E. Philbin and D.R. Tyler, Inorg. Chem., 25 (1986) 2976.

[37] Typically, photon energies in the visible region would not be sufficient to induce carbonyl loss in organometallic compounds; however, in the case of 19e species, our results with $P(OMe)_3$ indicate the W-CO bonds are significantly weakened so CO loss from excitation in the visible region is reasonable.

Tables

Table 1. Calculated and observed CO vibrational frequencies (in cm^{-1}) of relevant species for the photochemistry of $[CpW(CO)_3]_2$ with Lewis bases PR_3 (R= OMe, Ph).[a]

	calculated	observed
anti-$[CpW(CO)_3]_2$ (**A**)	1892 (0.0), 1915 (0.2), 1924 (0.8), 1932 (0.0), 1968 (1.0), 2000 (0.0)[b]	1907, 1954
gauche-$[CpW(CO)_3]_2$	1902 (0.2), 1909 (0.3), 1937 (0.4), 1944 (0.0), 1970 (0.6), 2014 (0.4)[b]	2010
anti-$[CpW(CO)_3]_2^-$	1839 (0.1), 1842 (0.0), 1862 (0.0), 1869 (0.8), 1881 (1.9), 1940 (0.0)[b]	not observed
$CpW(CO)_3^-$ (18e, **E**)	1785 (0.6), 1786 (0.7), 1880 (0.4)[c]	1768, 1795
$CpW(CO)_3$ (17e, **B**)	1906 (0.6), 1907 (0.4), 1987 (0.3)[c]	1881, 1994
$CpW(CO)_3P(OMe)_3$ (19e, $\mathbf{C_1}$)	1867 (0.5), 1877 (0.4), 1961 (0.4)[c]	1854, 1967
$CpW(CO)_3P(OMe)_3^+$ (18e, $\mathbf{D_1}$)	1976 (0.5), 2000 (0.2), 2056 (0.3)[c]	1995, 2064
$CpW(CO)_2P(OMe)_3$ (17e, $\mathbf{F_1}$)	1847 (0.6), 1910 (0.3)[c]	1815, 1916
$CpW(CO)_2P(OMe)_3^-$ (18e, **I**)	1753 (0.6), 1815 (0.4)[c]	1714
$CpW(CO)_2(P(OMe)_3)_2^+$ (18e, **H**)	1913 (0.5), 1972 (0.1)[c]	1990
anti-$[CpW(CO)_2P(OMe)_3]_2$ ($\mathbf{G_1}$)	1839 (0.0), 1871 (0.7), 1882 (0.2), 1920 (0.0)[b]	1835, 1868
gauche-$[CpW(CO)_2P(OMe)_3]_2$ ($\mathbf{G_1}$)	1847 (0.2), 1862 (0.6), 1875 (0.0), 1928 (0.2)[b]	
$CpW(CO)_3PPh_3$ (19e, $\mathbf{C_2}$)	1844 (0.7), 1864 (0.2), 1947 (0.3)[c]	1855
$CpW(CO)_3PPh_3^+$ (18e, $\mathbf{D_2}$)	1965 (0.5), 1981 (0.2), 2040 (0.3)[c]	2055
$CpW(CO)_2PPh_3$ (17e, $\mathbf{F_2}$)	1830 (0.6), 1901 (0.3)[c]	not observed

[a] calculated frequencies are scaled by the factor 0.9614[20]; [b] basis set **I**, [c] basis set **II**; calculated intensities are normalized to the 1968 cm^{-1} mode of *anti*-$[CpW(CO)_3]_2$); for the first four rows in the table, observed frequencies are given for PPh_3 solutions.

Table 2. Relative yield of disproportionated product observed experimentally and predicted from the kinetic models for the radical and dimer mechanisms (refer to Schemes 1 and 3, respectively) for different $[CpW(CO)_3]_2$ (**A**) concentrations and laser photolysis fluences. Data sets (a), (b), and (c) correspond to the data displayed in Fig. 2, and changes in yield are normalized to data set (a).

data set	experiment	radical mechanism	dimer mechanism
(a)	1.0	1.0	1.0
(b)	1.1 ± 0.2	1.1	0.3
(c)	2.2 ± 0.2	3.2	1.2

Captions for Illustrations

Scheme 1. Ultrafast photo-induced disproportionation of $[CpW(CO)_3]_2$ with the Lewis base $P(OMe)_3$ [10,11].[a]

[a] brackets represent the solvent cage

Scheme 2. Ligand substitution with 19e intermediates $CpW(CO)_3P(OMe)_3$ from the photolysis of $[CpW(CO)_3]_2$ with the Lewis base $P(OMe)_3$ [12]. Relevant time-scales for each step in the reaction are given below the arrows.

Scheme 3. Photochemical disproportionation mechanism for $[CpM(CO)_3]_2$ (M = Mo, W) in Lewis bases PR_3 (R = alkyl, alkoxy, aryl, aryloxy) as proposed by Tyler [7,8]

Scheme 4. Photochemical disproportionation mechanism for $[CpW(CO)_3]_2$ with the Lewis base PPh_3.[a]

[a] brackets represent the solvent cage

Fig. 1. Time-resolved IR spectra in the CO stretching region on the microsecond time-scale for 1.0 M PPh_3 in 1 mM $[CpW(CO)_3]_2$ (**A**)

Fig. 2. Time-resolved IR spectra in the CO stretching region on the microsecond time-scale for 85 mM PPh_3 in various concentrations of $[CpW(CO)_3]_2$ (**A**) and with different laser photolysis fluences. (a) 1.5 mM **A** and 0.2 mJ, (b) 0.5 mM **A** and 1.6 mJ, (c) 1.5 mM **A** and 0.8 mJ.

Fig. 3. (a) Kinetic data for $CpW(CO)_3^-$ and fits to the kinetic model predicted by the dimer (red

line) and radical mechanisms (blue line). Error bars represent one standard deviation. (b) Plot of same data as in (a) but with the ordinate as 1/(ΔmOD − A), which will yield a straight line for the radical mechanism (see text for details).

Fig. 4. Time-resolved IR spectra in the CO stretching region on the (a) nanosecond and (b) microsecond time-scales for 1 M $P(OMe)_3$ in 1.5 mM **A**.

Fig. 5. Kinetic data for (a) the 19e species $\mathbf{C_1}$ and 17e species $\mathbf{F_1}$ on the nanosecond time-scale and (b) the ionic products **H** and **I** on the microsecond time-scale. Lines represent monoexponential fits to the data (see text) and data for **H** is scaled by a factor of four for clarity.

Fig. 6. DFT optimized structures for the 19e species (**C**) and ligand substitution 17e species (**F**) with the Lewis bases $P(OMe)_3$ and PPh_3. Hydrogen atoms on the Lewis bases are omitted for clarity.

Fig. 7. DFT optimized structures for 19e species with the Lewis bases PMe_3 and PBu_3. Hydrogen atoms on the Lewis bases are omitted for clarity.

Illustrations: (for reviewing purposes only)

Scheme 1:

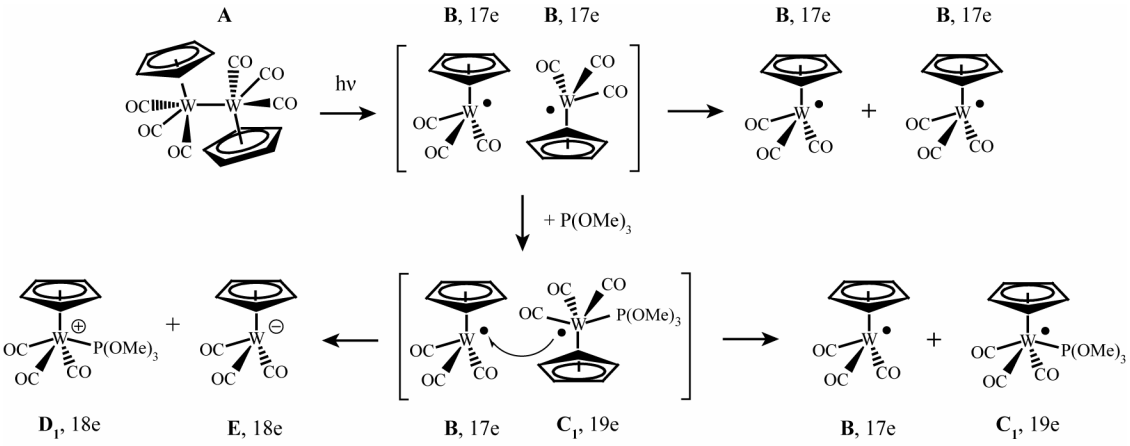

Scheme 2:

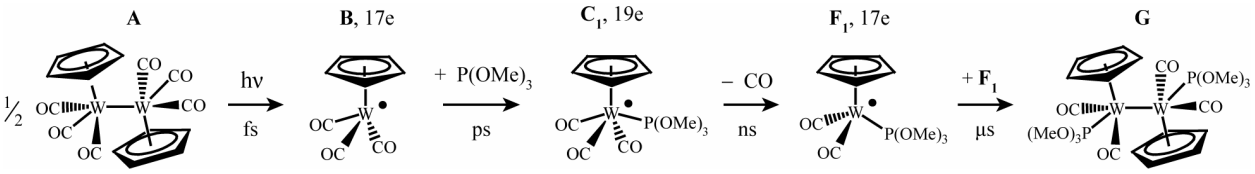

Scheme 3:

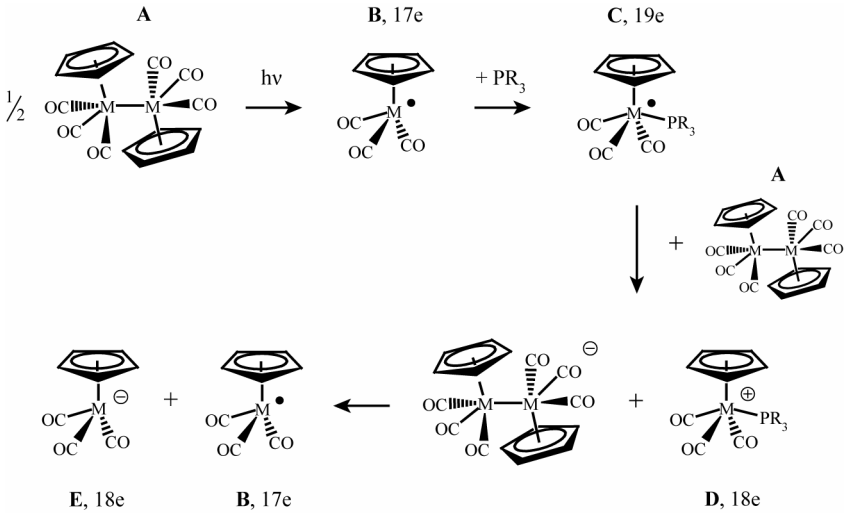

Scheme 4:

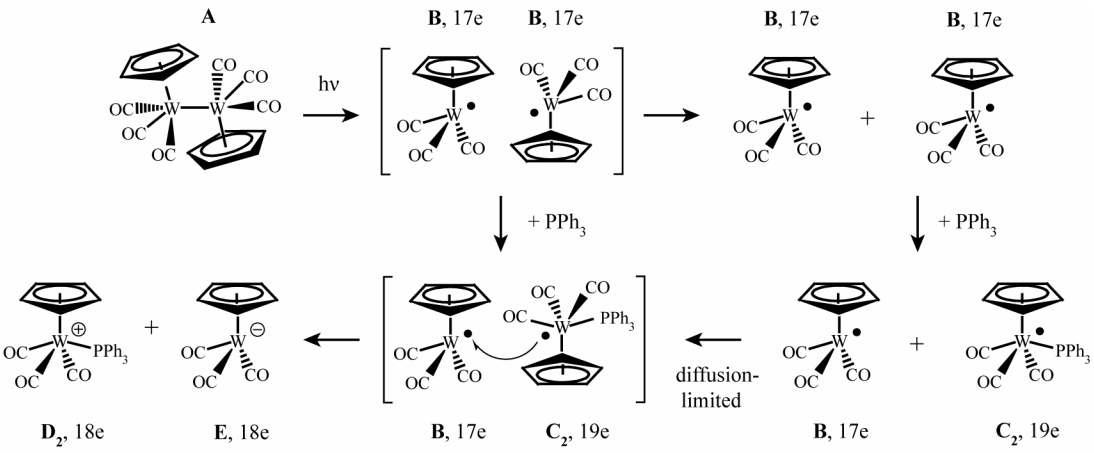
A
B, 17e
B, 17e
B, 17e
B, 17e
hν
+ PPh3
+ PPh3
diffusion-limited
D2, 18e
E, 18e
B, 17e
C2, 19e
B, 17e
C2, 19e

Fig. 1:

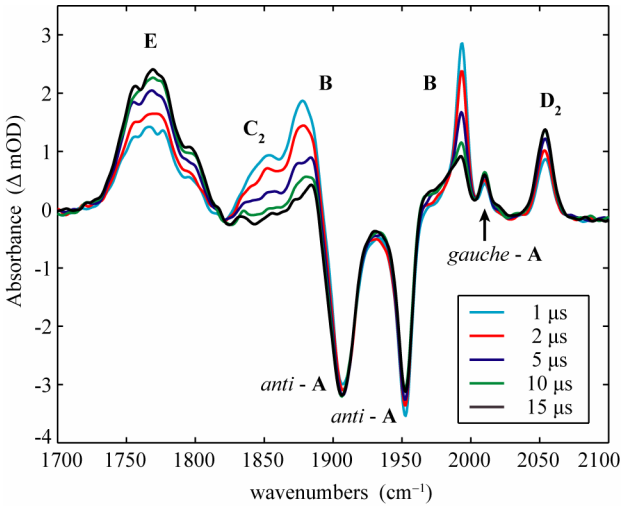
E
B
B
C2
D2
gauche - A
anti - A
anti - A
1 µs
2 µs
5 µs
10 µs
15 µs
Absorbance (Δ mOD)
wavenumbers (cm⁻¹)
3
2
1
0
-1
-2
-3
-4
1700
1750
1800
1850
1900
1950
2000
2050
2100

Fig. 2:

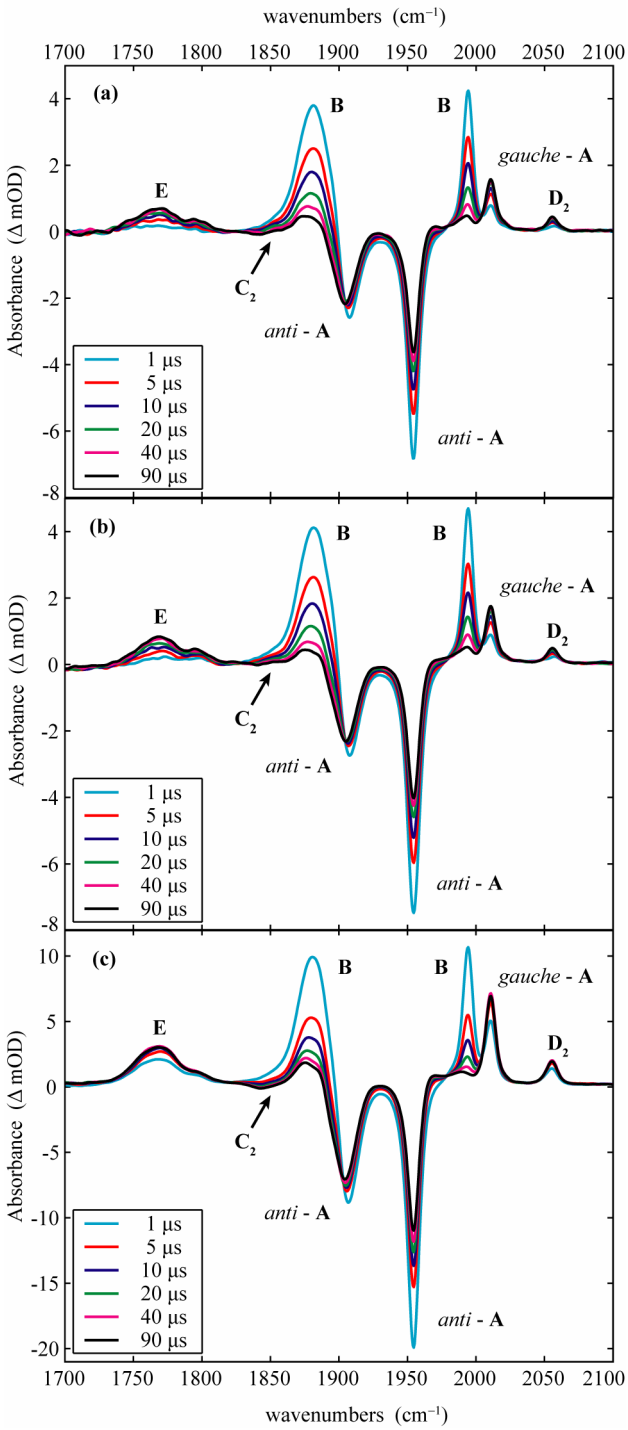
wavenumbers (cm⁻¹)
1700 1750 1800 1850 1900 1950 2000 2050 2100
(a)
(b)
(c)
Absorbance (Δ mOD)
B
B
gauche - A
E
D2
C2
anti - A
anti - A
1 µs
5 µs
10 µs
20 µs
40 µs
90 µs
wavenumbers (cm⁻¹)

Fig. 3:

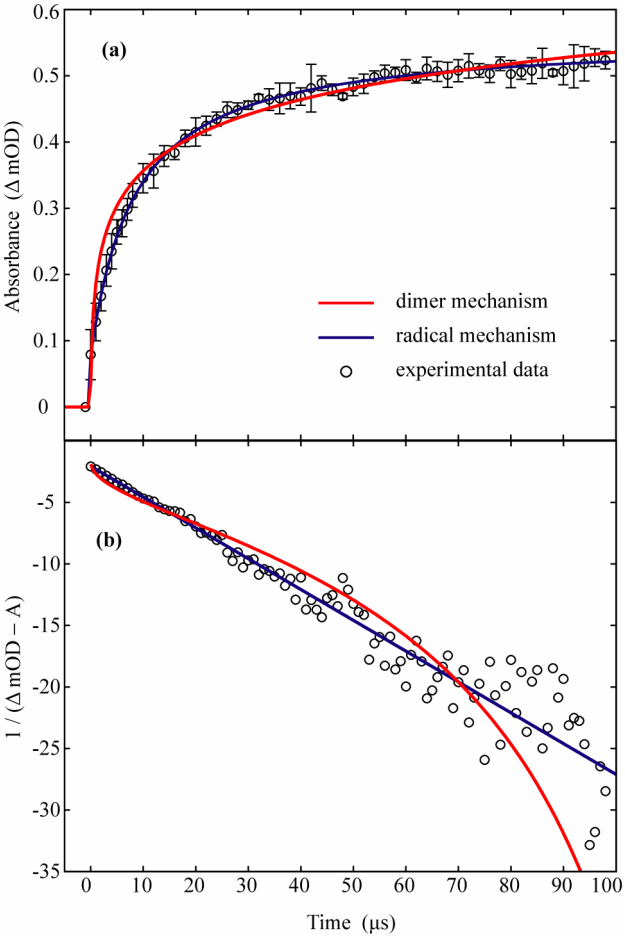
(a)
(b)
Absorbance (Δ mOD)
1 / (Δ mOD – A)
Time (μs)
dimer mechanism
radical mechanism
experimental data
0.6
0.5
0.4
0.3
0.2
0.1
0
-5
-10
-15
-20
-25
-30
-35
0
10
20
30
40
50
60
70
80
90
100

Fig. 4:

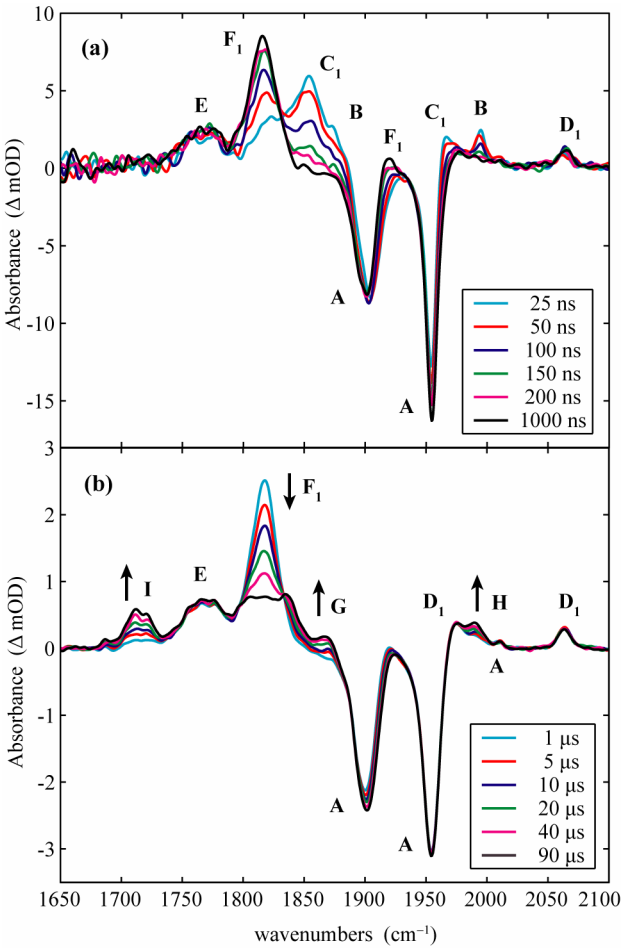
(a)
F1
C1
E
B
F1
C1
B
D1
A
A
25 ns
50 ns
100 ns
150 ns
200 ns
1000 ns
Absorbance (Δ mOD)
(b)
F1
I
E
G
D1
H
D1
A
A
A
1 µs
5 µs
10 µs
20 µs
40 µs
90 µs
Absorbance (Δ mOD)
wavenumbers (cm⁻¹)

Fig. 5:

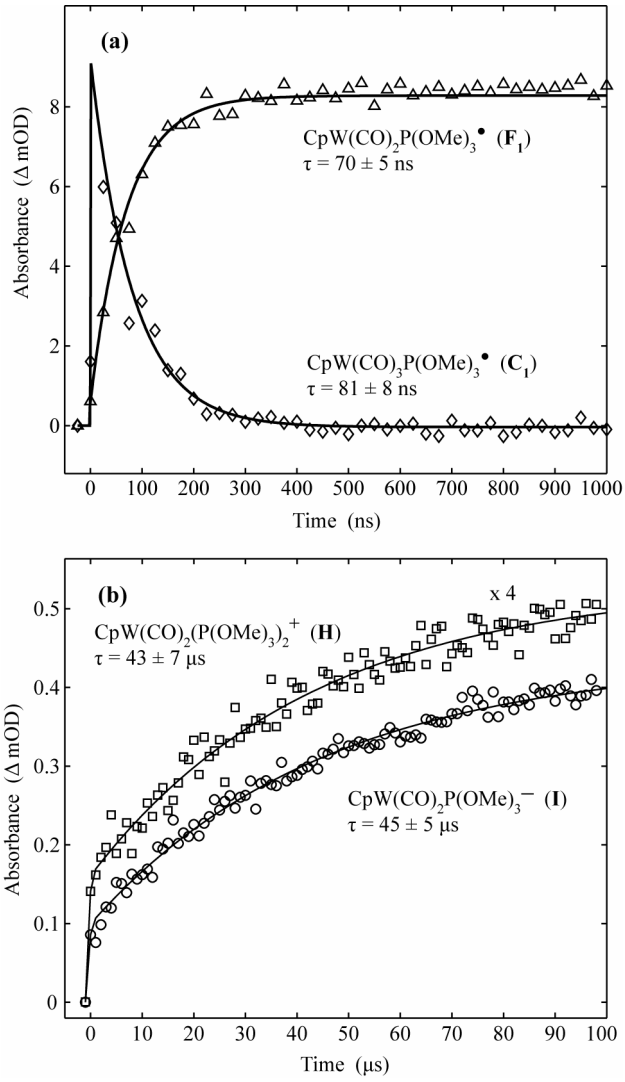
(a)
CpW(CO)2P(OMe)3• (F1)
τ = 70 ± 5 ns
CpW(CO)3P(OMe)3• (C1)
τ = 81 ± 8 ns
Absorbance (Δ mOD)
Time (ns)
(b)
x 4
CpW(CO)2(P(OMe)3)2+ (H)
τ = 43 ± 7 μs
CpW(CO)2P(OMe)3− (I)
τ = 45 ± 5 μs
Absorbance (Δ mOD)
Time (μs)

Fig. 6:

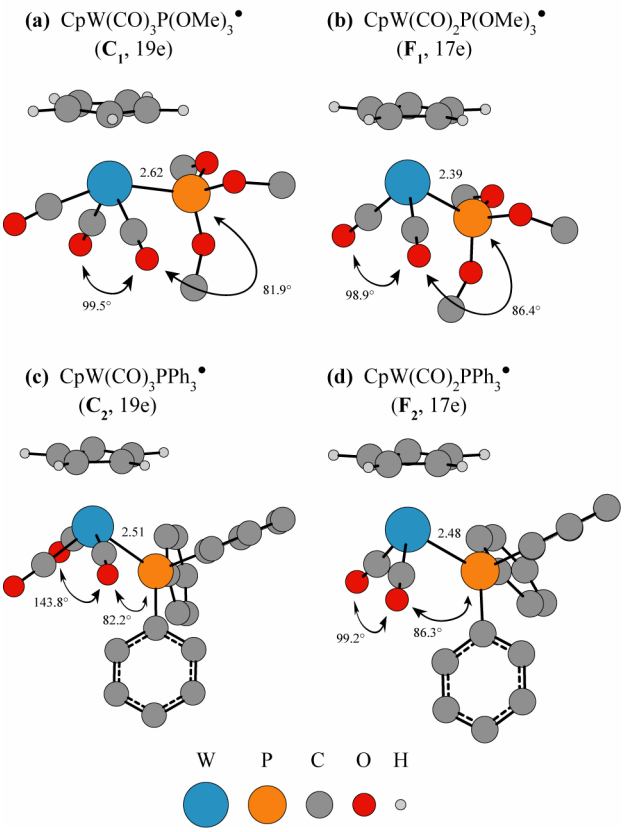
(a) CpW(CO)3P(OMe)3•
(C1, 19e)
2.62
99.5°
81.9°
(b) CpW(CO)2P(OMe)3•
(F1, 17e)
2.39
98.9°
86.4°
(c) CpW(CO)3PPh3•
(C2, 19e)
2.51
143.8°
82.2°
(d) CpW(CO)2PPh3•
(F2, 17e)
2.48
99.2°
86.3°
W P C O H

Fig. 7:

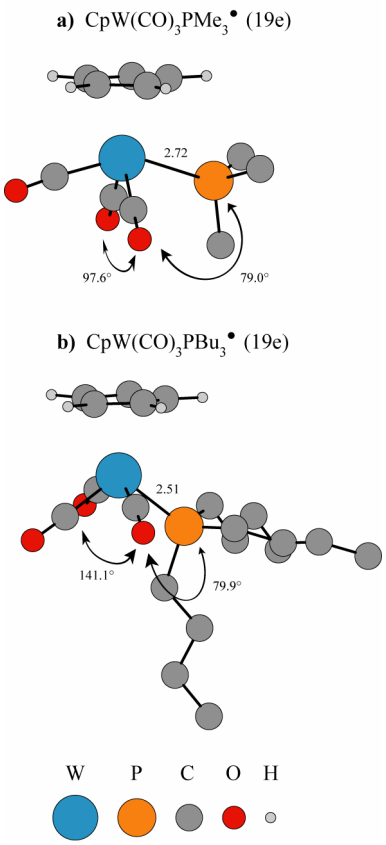
a) CpW(CO)3PMe3• (19e)
2.72
97.6°
79.0°
b) CpW(CO)3PBu3• (19e)
2.51
141.1°
79.9°
W
P
C
O
H